Letter

From orbital to paramagnetic pair breaking in layered superconductor 2*H*-NbS_2

D. Pizzirani,[1,2,*] T. Ottenbros,[1,2,*] M. van Rijssel,[1,2] O. Zheliuk,[1,2] Y. Kreminska,[3] M. Rösner,[2] J. F. Linnartz,[1,2] A. de Visser,[4] N. E. Hussey,[1,2,5] J. Ye,[3] S. Wiedmann,[1,2] and M. R. van Delft[1,2,†]

[1]*High Field Magnet Laboratory (HFML-EMFL), Radboud University, Toernooiveld 7, Nijmegen 6525 ED, The Netherlands*

[2]*Radboud University, Institute for Molecules and Materials, Nijmegen 6525 AJ, The Netherlands*

[3]*Device Physics of Complex Materials, Zernike Institute for Advanced Materials, University of Groningen, 9747 AG Groningen, The Netherlands*

[4]*Van der Waals-Zeeman Institute, University of Amsterdam, Science Park 904, 1098 XH Amsterdam, The Netherlands*

[5]*H.H. Wills Physics Laboratory, University of Bristol, Bristol BS8 1TL, United Kingdom*

(Received 4 April 2024; revised 15 July 2024; accepted 16 September 2024; published 7 October 2024)

The superconducting transition-metal dichalcogenides 2*H*-$NbSe_2$ and 2*H*-NbS_2 are intensively studied on account of their unique electronic properties such as Ising superconductivity, found in multi- and monolayers, with upper critical fields beyond the Pauli limit. Even in bulk crystals, there are reports of multiband superconductivity and exotic states, such as the Fulde-Ferrell-Larkin-Ovchinnikov phase. In this work, we investigate the superconducting properties of 2*H*-NbS_2 through a detailed high-field mapping of the phase diagram by means of magnetotransport and magnetostriction experiments. We compare the phase diagram between bulk crystals and a 6-nm-thick flake of 2*H*-NbS_2 and find a drastically enhanced Maki parameter in the flake, signifying a change of the relevant pair-breaking mechanism from orbital to paramagnetic pair breaking, which we attribute to an effect of enhanced spin-orbit coupling.

DOI: 10.1103/PhysRevResearch.6.L042006

The family of transition-metal dichalcogenides (TMDs) receives significant attention due to the tunability of its electronic ground states. TMDs, due to their van der Waals bound layers, can be exfoliated toward the atomic limit, enabling exotic physics such as Ising superconductivity [1–3]. This leads, for example, to a strong enhancement of the superconducting critical field of $NbSe_2$ upon thickness reduction due to the enhanced Ising spin-orbit coupling (SOC) effects. A particularly interesting pursuit within this field is the tuning of SOC through fabrication of TMD materials with few, even- or odd-numbered, layers [2]. Such tuning can profoundly affect the superconducting state in these compounds and is much sought after.

Within the TMD family, 2*H*-NbS_2 stands out as the only superconducting compound that does not exhibit a CDW even in monolayer form [4], despite indications that it may be close to a CDW transition [5–8]. Because of this, 2*H*-NbS_2 (we drop the 2*H* in the following) may provide a simpler platform than other TMDs to investigate the tunability of superconductivity based on odd/even numbers of layers. NbS_2 has a critical temperature T_c of approximately 6 K [9–12] and was reported to be a two-gap superconductor [11,13,14] and to exhibit orbital-selective two-dimensional superconductivity [15] as well as a Fulde-Ferrell-Larkin-Ovchinnikov (FFLO) state [16].

In this work, we investigate the superconducting pair-breaking mechanisms in bulk and thin-flake NbS_2 through a Werthamer-Helfand-Hohenberg (WHH) model description of their magnetic field-temperature (H-T) phase diagrams. Our magnetotransport measurements down to temperatures of 0.3 K and up to magnetic fields of 30 T allow us to determine the phase diagram over an unprecedented range as well as investigate the dimensionality of the superconducting state in this layered type-II superconductor.

We report a strong enhancement of paramagnetic pair breaking in thin-flake NbS_2, relative to the bulk material which is dominated by orbital pair breaking. This enhancement leads to a suppression of the upper critical field in the thin flake, in marked contrast to the enhanced critical fields seen in thin flakes of related materials such as $NbSe_2$ and TaS_2 [2]. We attribute our observations to an effect of spin-orbit coupling, leading to changes in scattering channels between bulk and thin-flake NbS_2. With this result, we take the first step toward thickness-controlled SOC in NbS_2.

Millimeter-size single crystals of NbS_2 were purchased from HQ Graphene and cut into bars approximately $3 \times 0.7 \times 0.03$ mm in size. Electrical contacts were subsequently made using silver paint (Dupont 4929). It was found that these contacts degrade over time, and had to be remade shortly before each experiment.

Thin flakes of NbS_2 were exfoliated by the standard scotch tape method in an inert argon atmosphere inside a glove box. The film was immediately protected by PMMA A4 photoresist and air exposure was minimized throughout the whole fabrication process. Electron beam lithography was used to

*These authors contributed equally.
†Contact author: maarten.vandelft@ru.nl

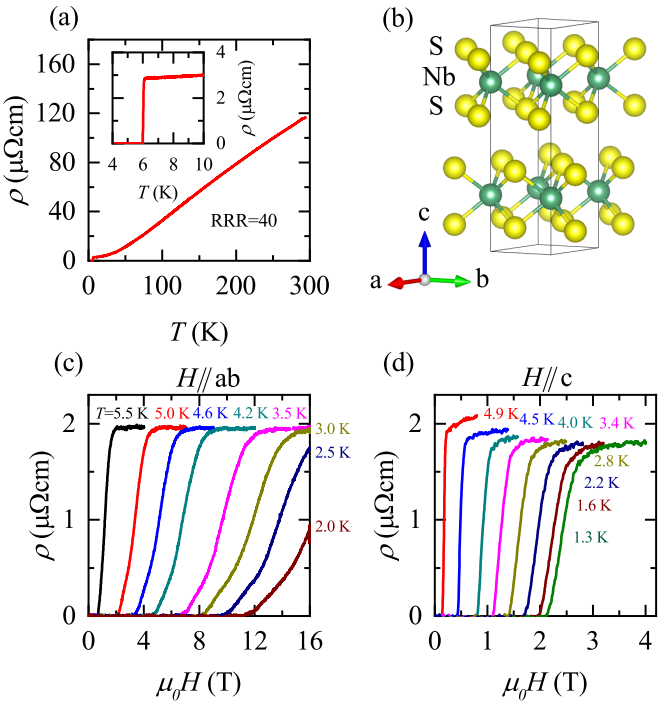

FIG. 1. (a) Temperature dependence of the resistivity in bulk NbS_2. The inset highlights the superconducting transition. (b) Crystal structure of NbS_2, with lattice parameters $a = b = 3.31$ Å and $c = 11.89$ Å [28]. Image generated with VESTA [29]. (c and d) Field-dependent resistivity at several temperatures, with the magnetic field applied (c) parallel (H // ab) and (d) perpendicular to the planes (H // c).

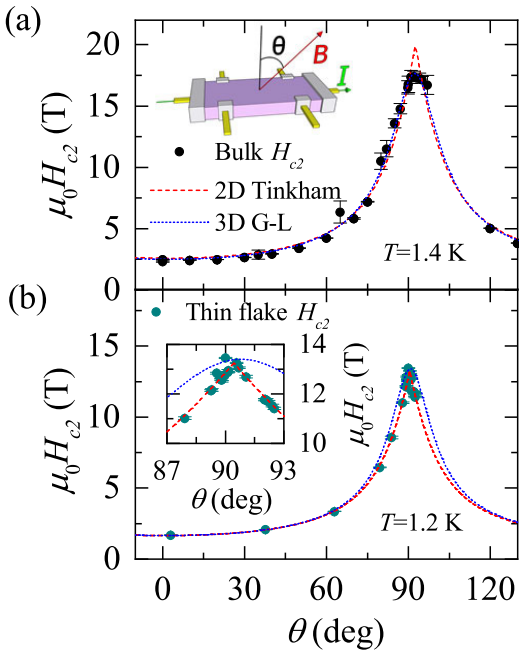

FIG. 2. (a) Critical field of bulk NbS_2 (defined as the field where the resistance reaches 50% of the normal state value) as a function of angle, at a temperature of 1.4 K. Dashed lines are fits to the two-dimensional Tinkham and three-dimensional Ginzburg-Landau models (see SM for the complete models [30]). Inset: configuration of the sample showing the field orientation. (b) Critical field of a 6-nm-thick NbS_2 thin flake as function of angle at $T = 1.2$ K, fit with the same models as (a). Inset: enlarged view of the region around 90°.

expose the electrode regions, followed by a metallization process with a Pt/Au film 5/40 nm thick. After liftoff and bonding, the sample was stored in vacuum prior to characterization.

Electrical magnetotransport measurements were performed in superconducting magnets up to 13 or 16 T and in a Bitter magnet up to 30 T using standard lock-in techniques and an applied current up to 1 mA for bulk samples and 10 μA for the thin flake.

Complementary measurements of the bulk thermodynamic properties were performed using a capacitive dilatometer technique [17] attached to an *in situ* rotation mechanism. Multiple single crystals were stacked together along the c axis and magnetic field up to 20 T was applied parallel to the planes. The magnetostriction curves were recorded with a capacitance bridge at a constant temperature using sweep rates of 1.0 T/min.

In Fig. 1(a), we show the temperature dependence of the resistivity of a typical bulk NbS_2 crystal. We identify a sharp superconducting transition (less than 0.15 K wide) around $T_c = 6$ K and, as expected, no resistive signature of a CDW transition as occurs in $NbSe_2$. The residual resistivity ratio (RRR) of our bulk samples is approximately 40, indicating that our material is of comparable quality to that used in previous reports [8,12,18–22].

Field-dependent data of the resistivity at different temperatures are plotted for magnetic fields parallel (H // ab, $\theta = 90°$) and perpendicular (H // c, $\theta = 0°$) to the crystal planes [see Fig. 1(b)] in Figs. 1(c) and 1(d), respectively. The main feature here is the increase in transition width with decreasing temperature that is especially pronounced in parallel fields. Such behavior is typically seen in two-dimensional (2D) superconductors [23–27]. The change in slope during the transition that also appears in the H // ab curves can be attributed to sample inhomogeneity.

The angle dependence of the critical field H_{c2} can be used to identify the dimensionality of the superconducting state. Before going into that, however, it is important to consider the definition of H_{c2}. There is no general agreement within the literature about which point should be used, but a common procedure is to consider the field at which a certain percentage (e.g., 90%) of the normal state resistance R_n is reached. An alternative method, especially useful when R_n cannot be unambiguously determined due to a limited field range of normal state resistivity or a large magnetoresistance, is to look at the first or second derivatives of the signal. Minima or maxima in these can then be used as consistent points to locate H_{c2}. In Fig. S1 in the Supplemental Material (SM) [30], we summarize the different definitions. We have employed all of these throughout our study, and found that they largely reproduce the same behavior. Within this paper, we use the 50%R_n criterion unless otherwise indicated.

In Figs. 2(a) and 2(b), we show the angle dependence of H_{c2} of a representative bulk NbS_2 sample and a 6-nm-thin flake, respectively. We attempt to describe the data using the

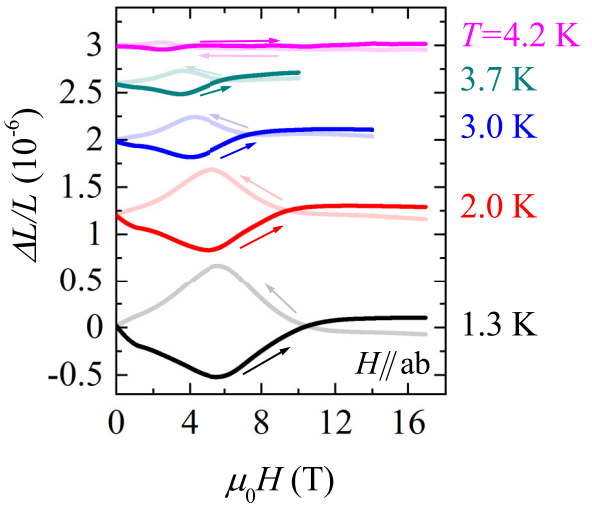

FIG. 3. Magnetostriction data of a stack of NbS_2 crystals in a parallel magnetic field at different temperatures. $\Delta L/L$ is the change in length relative to the original length. Arrows indicate whether the data was taken with increasing or decreasing magnetic field. Data are offset for clarity. The offsets between the increasing and decreasing field curves at maximal field are caused by eddy currents in the metallic parts of our capacitive dilatometer and are not intrinsic to the sample.

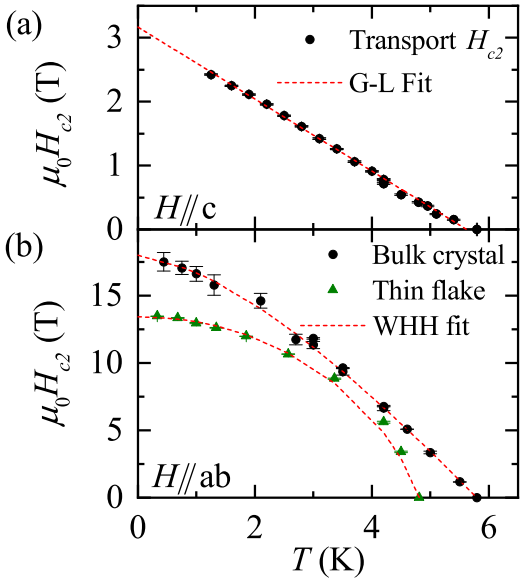

FIG. 4. (a) H-T phase diagram of bulk NbS_2 for $H \,//\, c$. The dashed line is a linear fit using the G-L model for a two-dimensional superconductor under perpendicular field. (b) Comparison of the phase diagrams for bulk and thin-flake NbS_2 (with $H \,//\, ab$). The WHH fit for the thin-flake data gives $\alpha_M = 6 \pm 1$ and $\lambda_{SO} = 1 \pm 0.3$.

Tinkham model [31] for 2D and the Ginzburg-Landau (G-L) model [32] for three-dimensional (3D) superconductors (corresponding equations can be found in the SM [30]). Clearly, 3D G-L provides a better description in the bulk case, particularly near $\theta = 90°$, suggesting that superconductivity is not confined to the individual layers, but a 3D state is formed instead. For the 6-nm-thin flake, on the other hand, the 2D model gives a better fit of the data, capturing the sharp cusp expected from the Tinkham model. This is somewhat surprising, as the sample thickness still exceeds the out-of-plane coherence length (of approximately 2 nm, as we will discuss later) and so this flake should normally be considered bulk despite being four orders of magnitude thinner than our actual bulk crystals.

The magnetostriction data obtained on bulk crystals are shown in Fig. 3 and demonstrate the expected behavior of a type-II superconductor in a magnetic field. As the field increases, the movement of magnetic flux lines is hindered by pinning, resulting in a compressive force [33]. Decreasing the field, on the other hand, leads to a tensile force, and this effect becomes stronger at lower temperatures. Beyond the field where the vortex lattice melts, no further effect of the magnetic field on the sample size is expected and the ratio of the change in length to the original length $\Delta L/L$ flattens out. As indicated in Fig. S5(b) of the SM [30], we can use this point to determine the irreversibility field H_{irr} for comparison with the corresponding field extracted from our transport measurements. The results of this comparison are shown in Fig. S6 of the SM [30] and demonstrate an excellent agreement. In this way, we support our transport experiments via a thermodynamic probe.

In the following, we analyze several aspects of the superconductivity in NbS_2. In particular, we discuss the question of dimensionality of the superconducting state and the manner of its breaking, for both bulk crystals and thin flakes.

In Figs. 4(a) and 4(b), we show the H-T phase diagrams of bulk NbS_2 for $H \,//\, c$ and $H \,//\, ab$, respectively. For $H \,//\, c$, the upper critical field depends linearly on temperature, matching the expectation for a 2D system in the Ginzburg-Landau model [34–36]. This suggests that the superconducting state in bulk NbS_2 may have a certain 2D character, at least under the influence of an out-of-plane applied magnetic field. Alternatively, $\mu_0 H_{c2}(T)$ may also flatten off below our measured temperature range. In that case, a two-gap model can explain the data [37], which would be consistent with previous reports of two-gap superconductivity in NbS_2 [13,14].

For $H \,//\, ab$, however, the G-L model [32], which does not capture Pauli limiting effects, cannot accurately describe the data (see Fig. S8 of the SM [30]). Instead, both H_{irr} and H_{c2} can be well described by the WHH model [38] that considers both Pauli paramagnetic and orbital effects, as shown in Fig. 4(b) (details of the WHH model can be found in the SM [30]).

In general, Cooper pairs in a superconductor may be broken either via the spin paramagnetic effect, where the magnetic field flips one spin of the spin-singlet Cooper pair to align both spins with the field direction, or via the orbital effect, where the Lorenz force exceeds the binding force between the electrons. Based on the WHH fitting, the spin paramagnetic effect is negligible in bulk NbS_2, as follows from the extracted value of the Maki parameter. We find that this parameter, which quantifies the relative strength of orbital and paramagnetic pair breaking, vanishes [i.e., $\alpha_M = \sqrt{2}\frac{H_{c2}^{orb}(0)}{H_{c2}^{pm}(0)} = 0$, where $H_{c2}^{orb}(H_{c2}^{pm})$ is the orbitally (paramagnetically) limited critical field]. From this we conclude that

orbital pair breaking is the dominant mechanism for breaking superconductivity in bulk NbS_2. This observation is inconsistent with the existence of an FFLO state in this material, which requires $\alpha_M > 1.8$ [39,40].

We now compare the H-T phase diagrams of bulk and thin-flake NbS_2. Clearly, both T_c and H_{c2} are reduced in the thin flake, but also the shape of the $\mu_0 H_{c2}(T)$ curve is notably different. Applying the WHH model to the thin-flake data, we find $\alpha_M = 6 \pm 1$ and $\lambda_{SO} = 1.0 \pm 0.3$, with the error bars estimated from the distribution of values found by fitting to different definitions of H_{c2} as well as the experimental determination of $\left(\frac{dH_{c2}}{dT}\right)_{T=T_c}$ (see Table S1 of SM [30]). This is a dramatic change compared to bulk NbS_2 and indicates a strong influence of Pauli paramagnetic pair breaking in addition to orbital pair breaking.

The key difference between our data and other reports [41,42] of increasing Maki parameter with decreasing material thickness is that we see a suppressed rather than increased H_{c2}, as could be understood from quenching of orbital pair breaking in a confined superconductor where screening currents cannot build up for $H \,//\, ab$ [41,42]. This is typically the case when a sample thickness of the order of ξ_c or smaller is realized, as the orbital pair-breaking effect should be absent when the thickness is smaller than the coherence length [43]. An increase of the Maki parameter with suppressed H_{c2} after thinning down a material has only been previously reported in FeSe flakes [44], though the effect was not explained and even bulk FeSe is Pauli limited, so the circumstances are notably different.

In order to investigate the possibility of quenched orbital pair breaking, we determine ξ for our samples. In general, ξ can be extracted from the orbital critical fields [32,44], giving $\xi_c = 1.9 \pm 0.2$ nm and $\xi_{ab} = 10.2 \pm 0.5$ nm for the bulk crystal (see SM [30]). Determining the same for the thin flake, however, requires knowledge of α_M in the in-plane and out-of-plane directions. Lacking $\alpha_M^{\perp}$ for the flake, we can only estimate a range of $\xi_c = 0.4$–2.5 nm (and $\xi_{ab} = 6$–14 nm) for $\alpha_M^{\perp} = 6$ - 0. In each case, ξ_c is smaller than the sample thickness of 6 nm, but some suppression of orbital pair breaking may still be expected if part of the sample is degraded and the effective superconducting thickness is less than 6 nm.

However, a suppression of orbital pair breaking alone cannot explain our data. If that were the main effect, it would lead to an enhancement of H_{c2} above that of the bulk crystals [41,42]. Instead, we see a reduction in H_{c2}. This suggests it is primarily an enhancement of paramagnetic pair breaking that is responsible for the larger α_M, such as might happen due to increased impurity scattering [45,46].

As an explanation for the enhanced paramagnetic pair breaking in our thin flake, we consider the mechanism discussed in Ref. [2] and worked out theoretically in Ref. [47]. This model primarily serves to explain the enhancement of H_{c2} due to Ising SOC seen in $NbSe_2$ or TaS_2, but also introduces a mechanism for the suppression of H_{c2}. This suppression arises from spin-orbit [2] and/or intervalley [47] scattering that can cause paramagnetic pair breaking. Specifically, the scattering between valleys requires a spin flip, and thus causes paramagnetic pair breaking. In this way, the Maki parameter increases.

In order to identify the origin of the difference between thin-flake and bulk NbS_2, we first consider the difference between the band structures of monolayer and bulk NbS_2 [48]. The most apparent difference is in the p_z states at the Γ point; in the monolayer, these are pushed below the Fermi energy. However, these states do not play a significant role in the superconductivity of NbS_2 [49]. Instead, we look to the other difference: the effect of spin-orbit coupling. As seen in the published band structures of Ref. [48], the effect of SOC is strongest near the K point. In bulk material, changes only take place away from the Fermi energy and no effects of SOC on the superconducting state are expected. In a monolayer, however, the band structure is affected by SOC even at the Fermi energy. Here, this causes singlet and triplet pairing channels to mix (as shown to occur in $NbSe_2$ [50,51]) and open up a new scattering channel as a result. This scattering leads to a further enhancement of paramagnetic pair breaking, in addition to that caused by impurity [45,46], spin-orbit [2], and intervalley [47] scattering, and thus increases α_M.

Of course, our thin flake is not a monolayer, but the spin-orbit coupling effects seen in monolayers are also expected to occur in few-layer samples with odd numbers of layers, as a result of inversion symmetry breaking [2]. As noted earlier, our thin-flake sample exhibits clear 2D behavior [see Fig. 2(b)] and may thus consist of less than 6 nm of superconducting NbS_2 (10 layers), with potentially an odd number of layers. This would be consistent with the oxidation of some of the layers, causing them to no longer be superconducting, as was previously seen in Ref. [19]. Furthermore, the spin-orbit scattering time in our flake is short ($\tau_{SO} = 186 \pm 78$ fs, see SM [30]), as extracted from the WHH fitting. This confirms that spin-orbit coupling is indeed strong and may be responsible for the observed changes in pair breaking. To definitively make this point, however, both theoretical and experimental work on a series of samples ranging from single layer to several layers will be required. This is beyond the scope of the present work.

We now investigate the Pauli limit of superconductivity, which was reported to be $H_{c2}^{pm} \approx 1.86 T_c = 10$–$11$ T [16] in NbS_2, a value exceeded by both our bulk and thin-flake samples. A possible explanation could lie in the existence of multigap superconductivity, a possibility that is also consistent with the observed temperature dependence of the critical field anisotropy [52,53] (see Fig. S7 of SM [30]). Via a different calculation of H_{c2}^{pm} as $H_{c2}^{pm} = \frac{\Delta}{\sqrt{g}\mu_B}$, with the g-factor $g = 2$ and the superconducting gap $\Delta = 1.2$ meV [13,14,54], this results in $\mu_0 H_{c2}^{pm} = 14.5$ T, below H_{c2} for bulk, but above it for the thin flake. Only the bulk crystal thus appears to violate the Pauli limit.

In 2D materials, the in-plane upper critical field can be enhanced beyond the Pauli limit due to Ising spin-orbit coupling [2,18], as has been reported for monolayer $NbSe_2$ [3,55]. This, however, appears unlikely to occur in bulk NbS_2 due to its significant interlayer coupling [18]. A violation of the Pauli limit may also occur in conjunction with a superconducting FFLO state, as was previously reported in NbS_2 [16] and $NbSe_2$ [56]. We note, however, that our data clearly exclude the existence of such a state in NbS_2. When entering an FFLO state, the resistive transition should become sharper [24], while we

observe the opposite [see Fig. 1(b)]. A sharp enhancement of H_{c2} and $H_{\rm irr}$ is also expected at low temperatures and field-angles very close to the in-plane direction [39], but is absent here. Finally, there is no sign of a transition between a conventional superconducting and an FFLO state in the magnetostriction.

The absence of FFLO in our samples could be attributed to the cleanliness of the crystals. In a clean superconductor, the mean free path λ exceeds the coherence length ξ, which is a requirement for the presence of an FFLO state. From our complementary Hall effect measurement (see Fig. S10 of SM [30]), we can estimate that $\lambda \approx 3$–6 nm (see SM for the calculation [30]), suggesting that the superconductivity in our bulk NbS_2 is in the dirty regime (i.e., $\lambda < \xi$). However, using a fitting procedure based on the parallel-resistor formalism (see SM and Fig. S11 [30]) [57], we instead obtain $\lambda \approx 13$ nm. We conclude that our bulk samples are in a crossover between the clean and dirty regimes. We cannot extract λ for the thin flake, but we note that even in clean films, surface scattering may destroy the FFLO state [43].

Considering the good agreement between our data and literature reports of RRR [8,12,20,21], resistivity [9,20,22], coherence length [15,22], carrier density [58,59], Fermi velocity [10], mobility [9], and the superconducting gap size [13,14,54], we conclude that our data present a consistent picture for superconductivity in NbS_2. We have thus established the complete H-T phase diagram of bulk NbS_2 through detailed magnetotransport and magnetostriction measurements and compared it with that of an exfoliated thin flake of NbS_2.

Our main finding, however, is a strongly enhanced Maki parameter with reduced H_{c2} in a thin flake compared to bulk NbS_2 crystals, suggesting a suppression of orbital pair breaking coupled with an enhancement of paramagnetic pair breaking. A possible explanation is spin-orbit coupling that affects few-layer NbS_2 flakes with odd layer numbers. Considering the unexpected two-dimensional behavior, this may be applicable to the thin-flake sample we have studied. Looking ahead, a systematic study of NbS_2 flakes with even and odd numbers of layers would allow us to understand the influence of spin-orbit coupling on the superconducting pair breaking in this material. By studying a wide range of thicknesses, it will be possible to identify the crossover regime where paramagnetic pair breaking begins to play a role. One may then think about purposely controlling the dominant pair-breaking mechanism, enabling a further understanding of these systems and greater control over their superconductivity. Furthermore, beyond the effect on superconductivity, the manipulation of spin-orbit coupling via thickness is an exciting prospect for two-dimensional van der Waals materials in general.

The authors acknowledge fruitful discussions with M. Katsnelson and would like to thank P. Tinnemans for XRD experiments. This work was supported by HFML-RU/NWO-I, member of the European Magnetic Field Laboratory (EMFL). This publication is part of the project TOPCORE (OCENW.GROOT.2019.048) of the research program NWO – GROOT, which is financed by the Dutch Research Council (NWO).

[1] B. T. Zhou, N. F. Q. Yuan, H. L. Jiang, and K. T. Law, Ising superconductivity and Majorana fermions in transition-metal dichalcogenides, Phys. Rev. B **93**, 180501(R) (2016).

[2] S. C. de la Barrera, M. R. Sinko, D. P. Gopalan,N. Sivadas, K. L. Seyler, K. Watanabe, T. Taniguchi, A. W. Tsen, X. Xu, D. Xiao, and B. M. Hunt, Tuning Ising superconductivity with layer and spin-orbit coupling in two-dimensional transition-metal dichalcogenides, Nat. Commun. **9**, 1427 (2018).

[3] Y. Xing, K. Zhao, P. Shan, F. Zheng, Y. Zhang, H. Fu, Y. Liu, M. Tian, C. Xi, H. Liu, J. J. Feng, X. X. Lin, S. Ji, X. Chen, Q. K. Xue, and J. Wang, Ising superconductivity and quantum phase transition in macro-size monolayer $NbSe_2$, Nano Lett. **17**, 6802 (2017).

[4] D. Lin, S. Li, J. Wen, H. Berger, L. Forró, H. Zhou, S. Jia, T. Taniguchi, K. Watanabe, X. Xi, and M. S. Bahramy, Patterns and driving forces of dimensionality-dependent charge density waves in 2H-type transition metal dichalcogenides, Nat. Commun. **11**, 2406 (2020).

[5] M. Leroux, M. Le Tacon, M. Calandra, L. Cario, M.-A. Méasson, P. Diener, E. Borrissenko, A. Bosak, and P. Rodière, Anharmonic suppression of charge density waves in 2H-NbS_2, Phys. Rev. B **86**, 155125 (2012).

[6] M. Leroux, L. Cario, A. Bosak, and P. Rodière, Traces of charge density waves in NbS_2, Phys. Rev. B **97**, 195140 (2018).

[7] R. Bianco, I. Errea, L. Monacelli, M. Calandra, and F. Mauri, Quantum enhancement of charge density wave in NbS_2 in the two-dimensional limit, Nano Lett. **19**, 3098 (2019).

[8] C. Wen, Y. Xie, Y. Wu, S. Shen, P. Kong, H. Lian, J. Li, H. Xing, and S. Yan, Impurity-pinned incommensurate charge density wave and local phonon excitations in 2H-NbS_2, Phys. Rev. B **101**, 241404(R), (2020).

[9] A. Majumdar, D. Vangennep, J. Brisbois, D. Chareev, A. V. Sadakov, A. S. Usoltsev, M. Mito, A. V. Silhanek, T. Sarkar, A. Hassan, O. Karis, R. Ahuja, and M. Abdel-Hafiez, Interplay of charge density wave and multiband superconductivity in layered quasi-two-dimensional materials: The case of 2H-NbS_2 and 2H-$NbSe_2$, Phys. Rev. Mater. **4**, 084005 (2020).

[10] V. G. Tissen, M. R. Osorio, J. P. Brison, N. M. Nemes, M. García-Hernández, L. Cario, P. Rodière, S. Vieira, and H. Suderow, Pressure dependence of superconducting critical temperature and upper critical field of 2H-NbS_2, Phys. Rev. B **87**, 134502 (2013).

[11] J. Kačmarčík, Z. Pribulová, C. Marcenat, T. Klein, P. Rodière, L. Cario, and P. Samuely, Specific heat measurements of a superconducting NbS_2 single crystal in an external magnetic field: Energy gap structure, Phys. Rev. B **82**, 014518 (2010).

[12] H. Lian, Y. Wu, H. Xing, S. Wang, and Y. Liu, Effect of stoichiometry on the superconducting transition temperature in single crystalline 2H-NbS_2, Physica C **538**, 27 (2017).

[13] I. Guillamón, H. Suderow, S. Vieira, L. Cario, P. Diener, and P. Rodière, Superconducting density of states and vortex cores of 2H-NbS_2, Phys. Rev. Lett. **101**, 166407 (2008).

[14] J. Kačmarčík, Z. Pribulová, C. Marcenat, T. Klein, P. Rodière, L. Cario, and P. Samuely, Studies on two-gap

superconductivity in $2H$-NbS_2, Physica C **470**, S719 (2010).

[15] X. Bi, Z. Li, J. Huang, F. Qin, C. Zhang, Z. Xu, L. Zhou, M. Tang, C. Qiu, P. Tang, T. Ideue, T. Nojima, Y. Iwasa, and H. Yuan, Orbital-selective two-dimensional superconductivity in $2H$-NbS_2, Phys. Rev. Res. **4**, 013188 (2022).

[16] C. Cho, J. Lyu, C. Y. Ng, J. Jun He, K. To Lo, D. Chareev, T. A. Abdel-Baset, M. Abdel-Hafiez, and R. Lortz, Evidence for the Fulde–Ferrell–Larkin–Ovchinnikov state in bulk NbS_2, Nat. Commun. **12**, 3676 (2021).

[17] R. Küchler, A. Wörl, P. Gegenwart, M. Berben, B. Bryant, and S. Wiedmann, The world's smallest capacitive dilatometer, for high-resolution thermal expansion and magnetostriction in high magnetic fields, Rev. Sci. Instrum. **88**, 083903 (2017).

[18] D. Huang, H. Nakamura, K. Küster, U. Wedig, N. B. M. Schröter, V. N. Strocov, U. Starke, and H. Takagi, Probing the interlayer coupling in $2H$-NbS_2 via soft-x-ray angle-resolved photoemission spectroscopy, Phys. Rev. B **105**, 245145 (2022).

[19] R. Yan, G. Khalsa, B. T. Schaefer, A. Jarjour, S. Rouvimov, K. C. Nowack, H. G. Xing, and D. Jena, Thickness dependence of superconductivity in ultrathin NbS_2, Appl. Phys. Express **12**, 023008 (2019).

[20] E. Martino, C. Putzke, M. König, P. J. W. Moll, H. Berger, D. LeBoeuf, M. Leroux, C. Proust, A. Akrap, H. Kirmse, C. Koch, S. N. Zhang, Q. S. Wu, O. V. Yazyev, L. Forró, and K. Semeniuk, Unidirectional Kondo scattering in layered NbS_2, npj 2D Mater. Appl. **5**, 86 (2021).

[21] B. Bag, D. J. Sivananda, P. Mandal, S. S. Banerjee, A. K. Sood, and A. K. Grover, Vortex depinning as a nonequilibrium phase transition phenomenon: Scaling of current-voltage curves near the low and the high critical-current states in $2H$-NbS_2 single crystals, Phys. Rev. B **97**, 134510 (2018).

[22] K. Onabe, M. Naito, and S. Tanaka, Anisotropy of the upper critical field in superconducting $2H$-NbS_2, J. Phys. Soc. Jpn. **45**, 50 (1978).

[23] J. Singleton, N. Harrison, C. H. Mielke, J. A. Schlueter, and A. M. Kini, A statistical model for the intrinsically broad superconducting-to-normal transition in quasi-two-dimensional crystalline organic metals, J. Phys.: Condens. Matter **13**, L899 (2001).

[24] S. Kasahara, Y. Sato, S. Licciardello, M. čulo, S. Arsenijević, T. Ottenbros, T. Tominaga, J. Böker, I. Eremin, T. Shibauchi, J. Wosnitza, N. E. Hussey, and Y. Matsuda, Evidence for an Fulde-Ferrell-Larkin-Ovchinnikov state with segmented vortices in the BCS-BEC-crossover superconductor FeSe, Phys. Rev. Lett. **124**, 107001 (2020).

[25] P. Szabó, P. Samuely, J. Kačmarčik, A. G. M. Jansen, A. Briggs, A. Lafond, and A. Meerschaut, Interlayer transport in the highly anisotropic misfit-layer superconductor (LaSe)1.14($NbSe_2$), Phys. Rev. Lett. **86**, 5990 (2001).

[26] J. L. Vicent, S. J. Hillenius, and R. V. Coleman, Critical-field enhancement and reduced dimensionality in superconducting layer compounds, Phys. Rev. Lett. **44**, 892 (1980).

[27] P. Baidya, D. Sahani, H. Kumar Kundu, S. Kaur, P. Tiwari, V. Bagwe, J. Jesudasan, A. Narayan, P. Raychaudhuri, and A. Bid, Transition from three- to two-dimensional Ising superconductivity in few-layer $NbSe_2$ by proximity effect from van der Waals heterostacking, Phys. Rev. B **104**, 174510 (2021).

[28] F. Jellinek, G. Brauer and H. Müller, Molybdenum and niobium sulphides, Nature (London) **185**, 376 (1960).

[29] K. Momma, and F. Izumi, VESTA 3 for three-dimensional visualization of crystal, volumetric and morphology data, J. Appl. Crystallogr. **44**, 1272 (2011).

[30] See Supplemental Material at http://link.aps.org/supplemental/10.1103/PhysRevResearch.6.L042006 for the models and calculations used for this work, as well as figures showing additional data.

[31] M. Tinkham, Effect of fluxoid quantization on transition of superconducting films, Phys. Rev. **129**, 2413 (1963).

[32] M. Tinkham, *Introduction to Superconductivity*, 2nd ed. (McGraw-Hill, New York, 1996).

[33] V. V. Eremenko, V. A. Sirenko, H. Szymczak, and A. Nabialek, Magnetostriction of superconductors (a review), Low Temp. Phys. **25**, 225 (1999).

[34] C. H. Sharma, A. P. Surendran, S. S. Varma, and M. Thalakulam, 2D superconductivity and vortex dynamics in $1T$-MoS_2, Commun. Phys. **1**, 90 (2018).

[35] J. M. Lu, O. Zheliuk, I. Leermakers, N. F. Q. Yuan, U. Zeitler, K. T. Law, and J. T. Ye, Evidence for two-dimensional Ising superconductivity in gated MoS_2, Science **350**, 1353 (2015).

[36] J. Zeng, E. Liu, Y. Fu, Z. Chen, C. Pan, C. Wang, M. Wang, Y. Wang, K. Xu, S. Cai, X. Yan, Y. Wang, X. Liu, P. Wang, S. J. Liang, Y. Cui, H. Y. Hwang, H. Yuan, and F. Miao, Gate-induced interfacial superconductivity in $1T$-$SnSe_2$, Nano Lett. **18**, 1410 (2018).

[37] X. Xing, W. Zhou, J. Wang, Z. Zhu, Y. Zhang, N. Zhou, B. Qian, X. Xu, and Z. Shi, Two-band and Pauli-limiting effects on the upper critical field of 112-type iron pnictide superconductors, Sci. Rep. **7**, 45943 (2017).

[38] N. R. Werthamer, E. Helfand, and P. C. Hohenberg, Temperature and purity dependence of the superconducting critical field, H_{c2}. III. Electron spin and spin-orbit effects, Phys. Rev. **147**, 295 (1966).

[39] J. Wosnitza, FFLO states in layered organic superconductors, Ann. Phys. **530**, 1700282 (2018).

[40] L. W. Gruenberg and L. Gunther, Fulde-Ferrell effect in type-II superconductors, Phys. Rev. Lett. **16**, 996 (1966).

[41] W. M. J. van Weerdenburg, A. Kamlapure, E. H. Fyhn, X. Huang, N. P. E. van Mullekom, M. Steinbrecher, P. Krogstrup, J. Linder, and A. A. Khajetoorians, Extreme enhancement of superconductivity in epitaxial aluminum near the monolayer limit, Sci. Adv. **9**, eadf5500 (2023).

[42] H. Nam, H. Chen, P. W. Adams, S.-Y. Guan, T.-M. Chuang, C.-S. Chang, A. H. MacDonald, and C.-K. Shih, Geometric quenching of orbital pair breaking in a single crystalline superconducting nanomesh network, Nat. Commun. **9**, 5431 (2018).

[43] Y. Matsuda and H. Shimahara, Fulde-Ferrell-Larkin-Ovchinnikov state in heavy fermion superconductors, J. Phys. Soc. Jpn. **76**, 051005 (2007).

[44] L. S. Farrar, M. Bristow, A. A. Haghighirad, A. McCollam, S. J. Bending, and A. I. Coldea, Suppression of superconductivity and enhanced critical field anisotropy in thin flakes of FeSe, npj Quantum Mater. **5**, 29 (2020).

[45] S. Khim, J. W. Kim, E. S. Choi, Y. Bang, M. Nohara, H. Takagi, and K. H. Kim, Evidence for dominant Pauli paramagnetic effect in the upper critical field of single-crystalline $FeTe_{0.6}Se_{0.4}$, Phys. Rev. B **81**, 184511 (2010).

[46] G. Fuchs, S. L. Drechsler, N. Kozlova, M. Bartkowiak, G. Behr, K. Nenkov, H. H. Klauss, J. Freudenberger, M. Knupfer, F. Hammerath, G. Lang, H. J. Grafe, B. Büchner, and L. Schultz,

Evidence for Pauli-limiting behaviour at high fields and enhanced upper critical fields near T_c in several disordered FeAs based superconductors, Physica C **470**, S288 (2010).

[47] S. Ilić, J. S. Meyer, and M. Houzet, Enhancement of the upper critical field in disordered transition metal dichalcogenide monolayers, Phys. Rev. Lett. **119**, 117001 (2017).

[48] C. Heil, M. Schlipf, and F. Giustino, Quasiparticle GW band structures and Fermi surfaces of bulk and monolayer NbS_2, Phys. Rev. B **98**, 075120 (2018).

[49] C. Heil, S. Poncé, H. Lambert, M. Schlipf, E. R. Margine, and F. Giustino, Origin of superconductivity and latent charge density wave in NbS_2, Phys. Rev. Lett. **119**, 087003 (2017).

[50] D. Wickramaratne, S. Khmelevskyi, D. F. Agterberg, and I. I. Mazin, Ising superconductivity and magnetism in $NbSe_2$, Phys. Rev. X **10**, 041003, (2020).

[51] M. Kuzmanović, T. Dvir, D. Leboeuf, S. Ilić, M. Haim, D. Möckli, S. Kramer, M. Khodas, M. Houzet, J. S. Meyer, M. Aprili, H. Steinberg, and C. H. L. Quay, Tunneling spectroscopy of few-monolayer $NbSe_2$ in high magnetic fields: Triplet superconductivity and Ising protection, Phys. Rev. B **106**, 184514 (2022).

[52] S. Khim, B. Lee, J. W. Kim, E. S. Choi, G. R. Stewart, and K. H. Kim, Pauli-limiting effects in the upper critical fields of a clean LiFeAs single crystal, Phys. Rev. B **84**, 104502 (2011).

[53] A. Gurevich, Enhancement of the upper critical field by nonmagnetic impurities in dirty two-gap superconductors, Phys. Rev. B **67**, 184515 (2003).

[54] P. Diener, M. Leroux, L. Cario, T. Klein, and P. Rodière, In-plane magnetic penetration depth in NbS_2, Phys. Rev. B **84**, 054531 (2011).

[55] X. Xi, Z. Wang, W. Zhao, J. H. Park, K. T. Law, H. Berger, L. Forró, J. Shan, and K. F. Mak, Ising pairing in superconducting $NbSe_2$ atomic layers, Nat. Phys. **12**, 139 (2016).

[56] P. Wan, O. Zheliuk, N. F. Q. Yuan, X. Peng, L. Z., M. Liang, U. Zeitler, S. Wiedmann, N. Hussey, T. T. M. Palstra, and J. Ye, Orbital Fulde–Ferrell–Larkin–Ovchinnikov state in an Ising superconductor, Nature (London) **619**, 46 (2023).

[57] R. A. Cooper, Y. Wang, B. Vignolle, O. J. Lipscombe, S. M. Hayden, Y. Tanabe, T. Adachi, Y. Koike, M. Nohara, H. Takagi, C. Proust, and N. E. Hussey, Anomalous criticality in the electrical resistivity of $La_{2-x}Sr_xCuO_4$, Science **323**, 603 (2009).

[58] J. Molenda, T. Bak, and J. Marzec, Electrical and electrochemical properties of niobium disulphide, Phys. Status Solidi A **156**, 159 (1996).

[59] M. Naito and S. Tanaka, Electrical transport properties in $2H$-NbS_2, -$NbSe_2$, -TaS_2 and -$TaSe_2$, J. Phys. Soc. Jpn. **51**, 219 (1982).